Microresonator Brillouin laser and multi-Stokes generation at 2 μm

Kanad Pathak, Satyam Puri, and Ravi Pant*
Laboratory for Phoxonics and Nonlinear Optics in Nanostructures (PHONON Lab), School of Physics, Indian Institute of Science Education and Research (IISER), Thiruvananthapuram, Kerala-695551, India

(Received 18 December 2023; revised 23 February 2024; accepted 21 March 2024; published 18 April 2024)

Brillouin scattering in microresonators has emerged as the driving process for developing high-coherence lasers for applications such as coherent optical communications, optical atomic clocks, microcomb solitons, and quantum communications. However, most of the demonstrations of microresonator Brillouin lasers have been limited to a 1550 nm wavelength regime, which benefits from the development of low-loss microresonator devices on different material platforms and the availability of tunable pump lasers. The development of wide bandwidth thulium-doped fiber amplifiers and low two-photon absorption in silicon around 2 μm makes this wavelength region a potential candidate for applications in future optical communications, gravitation wave sensing, and atmospheric sensing. All these applications will benefit from the development of Brillouin lasers. However, there has not been much progress on microresonator-based 2 μm Brillouin lasers. Here, we present a demonstration of a 2 μm microresonator Brillouin laser. We use whispering gallery mode resonances in a ∼330 μm silica microsphere to demonstrate a Brillouin lasing threshold of 35 mW. We achieve generation of second- and third-order Brillouin Stokes using pump powers of ∼60 mW and 104 mW, respectively. By tuning the pump laser wavelength, we demonstrate high-resolution (∼10 pm) tuning of the Brillouin laser. From the beat signal of the first- and third-order Brillouin Stokes, we estimate a Brillouin laser linewidth of ∼135 kHz, which is 15 times smaller than the pump linewidth. This work may find applications in optical communications, soliton combs, and atmospheric sensing in the 2 μm wavelength region.

DOI: 10.1103/PhysRevResearch.6.023062

Over the past decade, the wavelength region around 2 μm has attracted significant interest due to its applications in gravitational wave detection [1–3], free-space and fiber optic communications [4], gas sensing [5,6], and LIDAR [7]. With a continuous increase in the data demand, a "capacity crunch" [8] is imminent for the existing optical communication systems operating at 1.55 μm, which have already achieved a transmission capacity close to the nonlinear Shannon limit [9,10]. One way to alleviate this capacity crunch is to explore optical communication using other wavelength regions [11]. The development of wide bandwidth (∼200 nm) thulium-doped fiber amplifiers (TDFAs) and low-loss hollow core fibers [12] makes the 2 μm wavelength window a potential candidate for future optical communications along with 1.55 μm [11]. On the other hand, low two-photon absorption and high transparency of silicon in the 2 μm spectral window makes it useful for low vibration LIGO mirrors [13], which are to be used in the next-generation gravitational wave detectors [14] and integrated photonics research [15]. Many of these applications in the 2 μm wavelength region require high coherence continuous-wave (CW) lasers.

Lasers based on Brillouin gain resonance have emerged as a leading candidate for high coherence lasers across different wavelength regimes [16–19]. Most of the demonstrations of Brillouin lasers on fiber, high-Q microresonators, and integrated photonic platforms have been centered around ∼1.55 μm [20–30]. Recently, there have been demonstrations of visible lasers based on Brillouin scattering on a variety of platforms [19,31–33]. However, demonstrations of microresonator-based Brillouin lasers in the 2 μm spectral window have been lacking. In the few studies that have been performed in this wavelength region, the focus has been on stimulated Brillouin scattering (SBS) in fiber platforms. In [34], large Brillouin nonlinearity (∼100 x silica) and low loss of chalcogenide glasses in the 2 μm wavelength region was exploited to achieve low threshold (∼50 mW) Brillouin lasing in a 1.5-m-long suspended-core chalcogenide fiber. Brillouin fiber lasers at 2 μm have also been demonstrated using hundreds-of-meters-long standard single-mode fiber (SMF) [35] and 100-m-long speciality silica fibers (SMF1950) [36], where threshold pump powers of 650 and 100 mW, respectively, were used due to high loss (∼20 dB/km) of silica at 2 μm. The threshold for Brillouin lasing in a silica platform can be brought down by exploiting the large quality factor of whispering gallery modes in silica-based microresonators, which also allow integration with existing optical fiber systems through the coupling taper.

Here, we harness high-Q whispering gallery mode (WGM) resonances in a silica microsphere to report a demonstration of a low threshold (35 mW) 2 μm microresonator

*rpant@iisertvm.ac.in

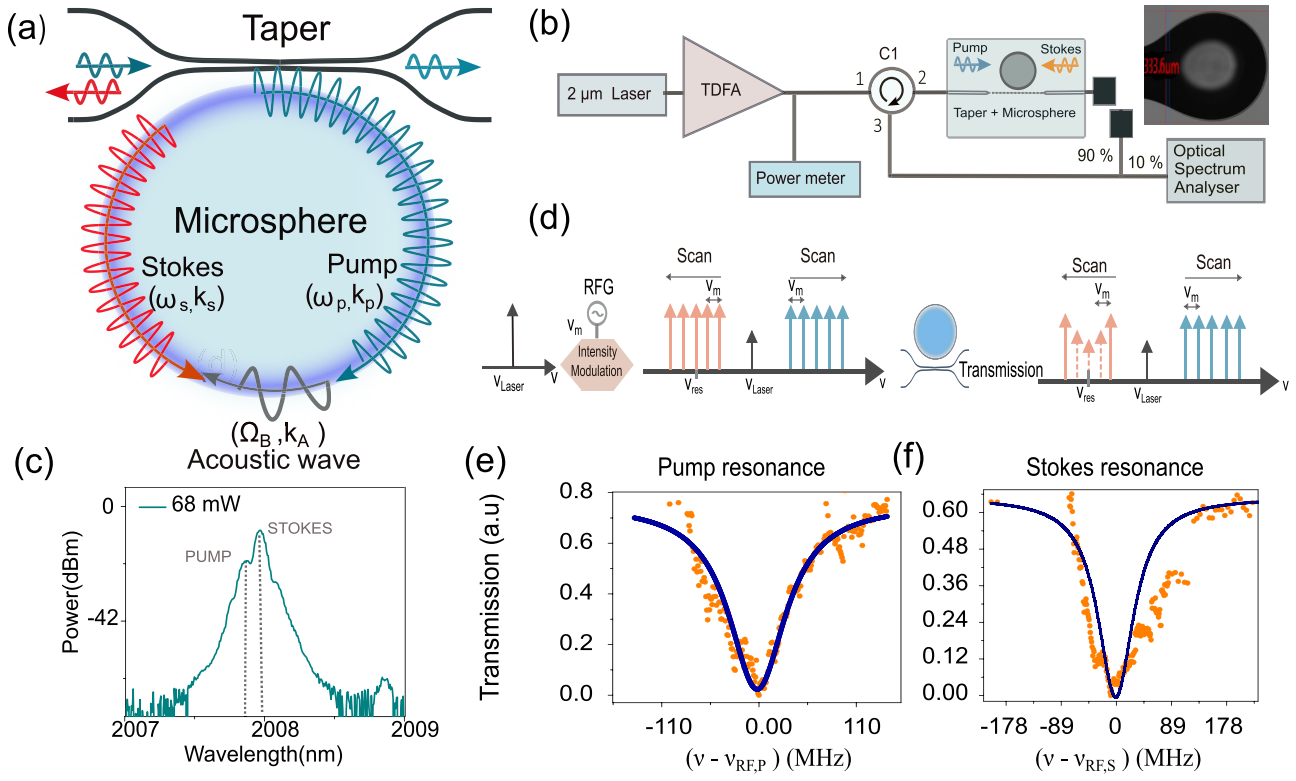

FIG. 1. Concept of 2 μm Brillouin lasing in a microresonator and resonance characterization. (a) Diagram illustrating Brillouin scattering in a microsphere. The angular frequencies of the pump, Stokes, and the acoustic wave are denoted by ω_p, ω_s, and Ω_B, respectively, while k_p, k_s, and k_A denote the wave numbers for the same. (b) Experimental setup utilized to realize Brillouin lasing. The inset shows the image of the microsphere. TDFA-thulium-doped fiber amplifier. (c) Demonstration of Brillouin-Stokes lasing at 2008 nm. (d) Schematic illustrating the side-band scan process. After intensity modulation of the laser, one of the sidebands is swept across the target microsphere resonance by varying the modulation frequency (e) pump and (f) Stokes resonance characterizations corresponding to (c).

Brillouin laser with an estimated narrow linewidth ∼135 kHz. By feeding back the first-order Stokes to the silica microsphere from the transmitted pump side, we made a composite fiber-microsphere ring cavity with a total silica fiber length ∼10 m, and we achieved a Brillouin lasing threshold of 35 mW, which is almost 30 times lower than the lasing threshold (∼1 W) for a Brillouin fiber ring laser made from a similar length (14 m) silica fiber [37]. We achieve excitation of the second- and third-order Stokes with threshold powers of 60 mW and ∼104 mW, respectively, when the first-order Brillouin Stokes signal is fed back to the microsphere. By varying the pump laser wavelength, we realize high-resolution tuning (∼10 pm) of the Brillouin laser. We study the stability of the Brillouin laser and achieve stable operation for more than an hour. Demonstration of a low-threshold 2 μm Brillouin laser in a silica microresonator opens up opportunities to realize intracavity pumped 2 μm Kerr and soliton combs [38,39] for applications in optical communications, dual-comb spectroscopy, gas sensing, and their integration with existing fiber-based systems.

I. RESULTS

Figure 1(a) illustrates the process of Brillouin scattering inside a whispering gallery microresonator. The incident pump wave of frequency (ω_p) gets reflected off a copropagating acoustic wave of frequency (Ω_B) and generates a counter-propagating Stokes signal (ω_s), which is downshifted from the pump by the frequency of the acoustic wave $\omega_s = \omega_p - \Omega_B$. This process takes place in accordance with energy and momentum conservation $k_p - k_s = K_A$, where k_p, k_s, and K_A are the wave vectors for the pump, Stokes, and the acoustic wave. While the energy conservation demands that the Stokes frequency is downshifted from the pump frequency by the acoustic wave frequency, momentum conservation relates the pump wavelength λ_p and acoustic frequency $\nu_B = \frac{\Omega_B}{2\pi}$ according to [40]

$$\nu_B = \frac{2nV_a}{\lambda_p}, \tag{1}$$

where n is the refractive index of the optical mode at the pump frequency, and V_a is the speed of sound in the material. Using $V_a = 5972$ m/s, $n = 1.438$, the estimated Brillouin shift at $\lambda_p \sim 2007$ nm is ∼8.55 GHz. For efficient Brillouin lasing, it is essential that the pump and Stokes signals coincide with the cavity resonances. In this work, we use a silica microsphere with a diameter d of 330 μm, which corresponds to a free spectral range (FSR $= \frac{c}{2\pi nr}$) of ∼200 GHz, where $r = \frac{d}{2}$, and c is the speed of light in vacuum. Since the estimated Brillouin shift is 8.55 GHz, the Stokes and the pump correspond to different mode families [41,42].

Figure 1(b) shows the experimental setup for realizing Brillouin lasing in a microsphere. A continuous-wave (CW) 2 μm laser (Eblana make) with a linewidth of ∼2 MHz is amplified

using a thulium-doped fiber amplifier and is coupled to the microsphere using a taper connected to port 2 of the circulator C1. The taper was fabricated by employing a differential pulling process in a Vytran GPX-3000 Glass processor. This was done in two steps to reduce the diameter from 125 μm to ∼1 μm. The microsphere was fabricated by heating a perfectly cleaved fiber end with the filament of the Glass processor. This allowed the fiber tip to melt and assume a spherical shape. The process was repeated until the target diameter was achieved. The TDFA output is split using a 99/1 coupler, where the 1% port is used to monitor the input power. The reflected signal collected at port 3 of the circulator is further split by a 90/10 splitter, where the 10% port is used to measure the backreflected optical spectrum and the 90% port is used for measuring the radiofrequency spectrum and studying the effect of Stokes feedback on the Brillouin lasing threshold. Figure 1(c) plots the measured backscattered optical spectrum showing the Rayleigh scattered pump and generated Stokes signal for an input power of ∼68 mW. Since our laser has a coarse tuning resolution, we characterize the Q-factor of the pump and Stokes resonance by intensity modulation of the 2 μm laser and scanning the modulation sideband across the pump and the Stokes resonance, as shown in Fig. 1(d). By measuring the transmitted power of the modulation sideband on the optical spectrum analyzer (OSA) as a function of the modulation frequency (tuned in steps of ∼1 MHz), we obtain Figs. 1(e) and 1(f) for the pump and Stokes resonance, respectively. From Figs. 1(e) and 1(f), we estimate a full width at half-maximum (FWHM) bandwidth of 78 and 70 MHz for the pump and Stokes resonance, respectively, resulting in quality factors of 1.9 and 2.1 Million. $\nu_{RF,(P,S)}$ denoted in Figs. 1(e) and 1(f) refer to the modulation frequency at which the sideband showed minimum transmission for pump and Stokes resonances, respectively.

Threshold study: The threshold power required for Brillouin scattering in a microsphere is given by [28]

$$P_{\text{threshold}} = \left(\frac{\pi^2 n^2 V}{Bg\lambda_p\lambda_s Q_p Q_s}\right)\left(\frac{1}{1+\frac{Q_m\Lambda_m}{2\pi r}}\right). \tag{2}$$

Here, V is the optical-mode volume for the pump, and B is the modal overlap factor between the pump mode, the Stokes mode, and the mechanical mode. $Q_{p,s,m}$ are the quality factors at the pump (λ_p), Stokes (λ_s), and mechanical mode (Λ_m) wavelengths, and r and g stand for the microsphere radius and the Brillouin gain coefficient, respectively. We use the COMSOL MULTIPHYSICS solver [43] to calculate the optical and mechanical modes, B and V (see the Appendix), for a microsphere with $d = 330$ μm at the pump and Stokes wavelengths, shown in Fig. 1. Using these quantities in Eq. (2), we estimate a threshold of ∼9 mW.

To determine the Brillouin lasing threshold, we measure the backscattered spectra at different pump powers in the absence and presence of Stokes feedback, where a part of the backscattered signal is fed back to the microsphere using a fiber ring. The backscattered signal at port 3 of C1 and the transmitted signal at the output port of the taper are each connected to 90/10 couplers [see Fig. 2(a)]. To realize Stokes feedback, 90% of the backscattered signal is then connected to the 90% port of the coupler at the taper transmission side. The 10% ports of the couplers in the transmission and backscattered direction are used for measuring the optical spectra at different pump powers.

Figures 2(b)–2(e) plot the Stokes power for different Stokes orders, along with the corresponding optical spectra (see the inset), as a function of the pump power (P_p). The Stokes power is obtained from the spectra shown in the inset. The pump power P_p for these plots is obtained by subtracting the circulator loss (around 1.7 dB), taper transition loss, and transmitted pump power from the input laser power measured at the 1% port of a 99/1 coupler at the output of the TDFA [see Fig. 2(a)]. The transmitted pump power is estimated based on the optical spectra for the second-order Stokes in Fig. 2(d). The taper loss changed from −0.14 to −1.7 dB during the measurements and is accounted accordingly for threshold measurements. Figure 2(b) plots the power (P_{S1}) of the first-order Stokes (S1) as a function of the pump power. The optical spectra in the inset of Fig. 2(b) are measured on the OSA, which is connected to the 10% port of the splitter connected to port 3 of the circulator C1. From a linear fit to the experimentally measured P_{S1}, we obtain a threshold of 40 mW in the absence of feedback.

To study the effect of Stokes feedback on the lasing threshold, we measure the backscattered spectra [see Fig. 2(c)] in the presence of Stokes feedback for different input pump powers. The 90% ports of the fiber splitters on the transmitted and reflected sides were connected to form the feedback loop, and the spectra were observed at the 10% port of the backscattered signal. From the fit to the measured data in Fig. 2(c), we obtain a lasing threshold of 35 mW. Here, the pump wavelength was shifted by 0.18 nm with respect to the without-feedback case due to the effect of resonance shift because of the fiber ring cavity.

Since feedback reduces the threshold for Brillouin lasing, we conduct a higher-order Stokes generation study with Stokes feedback. Figure 2(d) plots the second-order Stokes power (P_{S2}), which is obtained from the measured forward spectra (see the inset) at the output of the taper, as a function of P_p. The forward spectra shown in the inset of Fig. 2(d) are collected at the 10% port. It shows the transmitted pump and excitation of the second-order Stokes (S2). From the corresponding threshold plot (P_{S2} versus P_p) in Fig. 2(d), we obtain a threshold of 60 mW for the second-order Stokes. A threshold of 104 mW was obtained for the third-order Stokes (S3) signal from the linear fit to the S3 power P_{S3} versus P_p plot, shown in Fig. 2(e). The corresponding reflected spectra, demonstrating the presence of the third-order Stokes, are shown in the inset. The threshold studies for the second- and third-order Stokes generation were performed at the pump wavelengths that result in low threshold for S2 and S3 generation.

Tuning and stability study: High-Q and discrete nature of the WGM resonances, and strict phase matching of the Brillouin scattering process imposes restrictions on the pump wavelength and microresonator design. For example, realizing the Brillouin laser in a microresonator with only the fundamental whispering gallery mode requires matching of the fundamental mode FSR with the Brillouin shift (Ω_B), which limits the tuning resolution of the Brillouin laser. Since the Brillouin shift in silica for a pump wavelength of 1550 nm is ∼11 GHz, matching of FSR with Ω_B necessitates

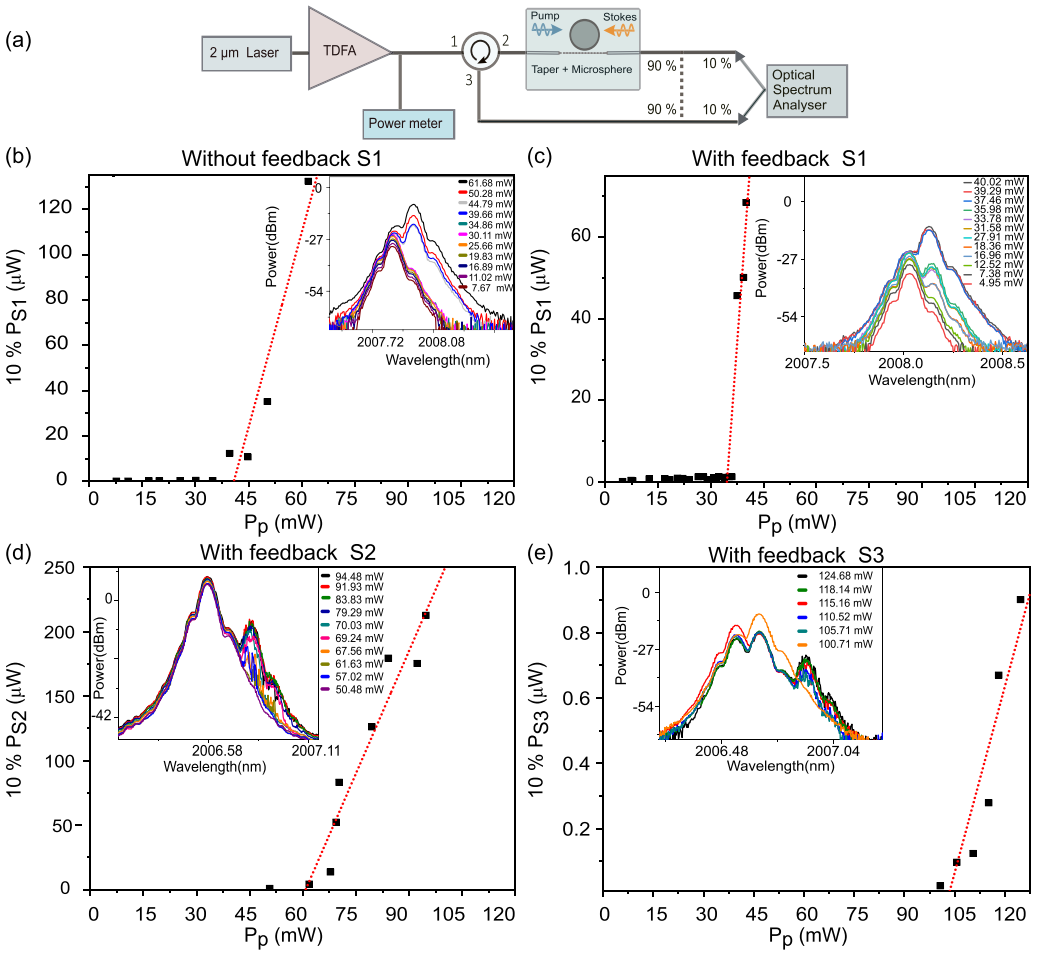

FIG. 2. Threshold study for Brillouin lasing and multi-Stokes generation: (a) Experimental design to observe Brillouin lasing in a silica microsphere with and without feedback. The feedback loop is completed upon connecting the 90% path, shown by dotted lines. Threshold study of Brillouin laser (b) without feedback and (c) with feedback, with the insets showing corresponding optical spectra. Panels (d) and (e) show the threshold study for the second- and third-order Stokes, respectively. The second-order Stokes signal is observed in the forward direction.

fabrication of a large-diameter (mm size) microresonator with strict fabrication tolerance, and access to a laser with fine tuning resolution. Tunable Brillouin lasers with a tuning range in excess of 10 nm around 1550 nm have been demonstrated in wedge microresonator, where matching of FSR and Ω_B is realized through precise fabrication [27]. Since the Brillouin shift reduces with the pump wavelength [see Eq. (1)], realization of a 2 μm Brillouin laser using microresonators with only the fundamental WGM requires fabrication of microresonators with diameter larger than that at 1550 nm due to the condition of matching FSR and Ω_B. Most of the demonstrations of tunable 2 μm Brillouin lasers, so far, have been realized in fiber-ring cavities, where the small FSR of the cavity allows many cavity modes within the Brillouin gain profile, and low finesse of the cavity enables better overlap of the pump with the resonance [44–46].

Microsphere-based WGM resonators, however, have many higher-order optical modes besides the fundamental mode. Even for microspheres with a diameter of ∼100 μm, there are many higher-order mode families [47,48], where each of the mode family has an FSR of ∼ hundreds of GHz. However, resonance frequencies of the whispering gallery modes from different families vary only slightly from each other, due to a small difference in their effective indices. The presence of many closely spaced cavity resonances belonging to different mode families allows alignment of the pump wavelength and the Brillouin gain resonance with one of these modes and thus enables tunable Brillouin lasers with a tuning step $< \Omega_B$.

Figure 3(a) shows the measured backscattered optical spectra of the Brillouin laser for different input pump wavelengths, demonstrating a tuning range of 1.8 nm, which is limited by the pump laser tunability. We achieve a tuning resolution ∼50 pm [see the inset Fig. 3(a)], which is nearly half of the measured Brillouin shift of 115 pm (∼8.58 GHz) at 2 μm [see Fig. 3(a), inset]. The presence of higher-order whispering gallery modes in a microsphere, therefore, enables tunable Brillouin lasers with a tuning step smaller than the Brillouin shift and the FSR of the modes, which is not possible in microresonators with only the fundamental WGM. Further, the presence of many higher-order modes removes the requirement of having large-diameter resonators for Brillouin lasing.

The wavelength tuning was achieved by adjusting the temperature of the Brillouin pump laser, which has a temperature

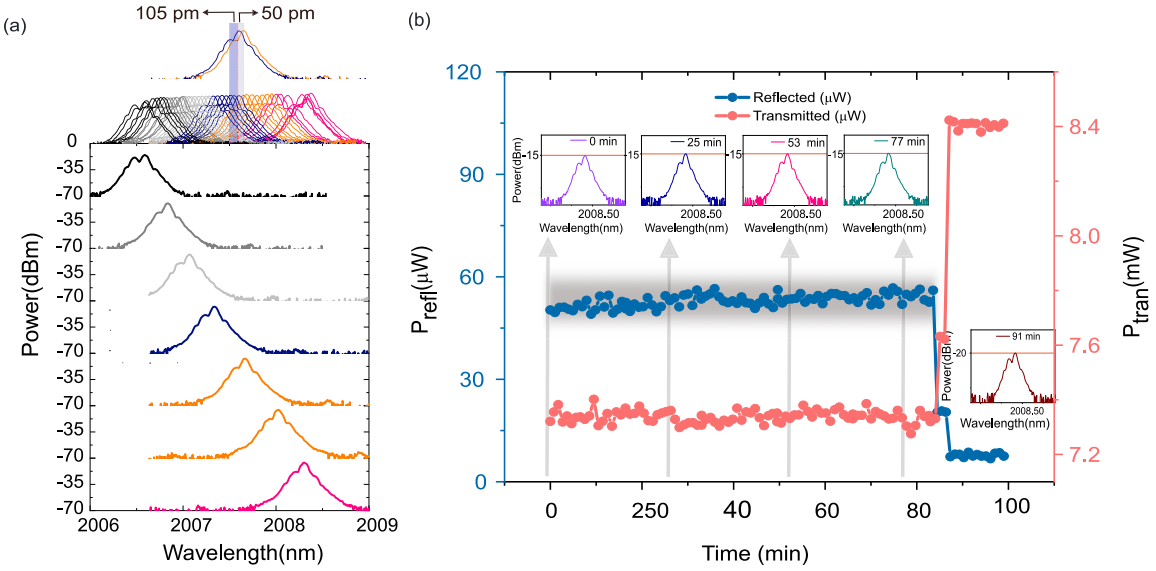

FIG. 3. Tuning and power stability: Top panel shows OSA traces at two successive pump wavelengths for Brillouin lasing, showing a measured tuning step of 50 pm (red dotted lines). The middle panel shows OSA traces for Brillouin lasing over the entire pump wavelength tuning range. The wavelength axis for the middle and the bottom panel is the same. The bottom panel shows plots of selected traces from the middle panel for better clarity. The tuning step of the Brillouin laser is limited by the wavelength tunability step (∼10 pm) of the pump laser, whereas the smallest measured tuning step is limited by the OSA resolution (50 pm). (b) Variation of reflected (blue) and transmitted (orange) power with time. OSA traces corresponding to certain time instances are shown in the insets. As the Stokes power (reflected: blue trace) reduces, the transmitted power (red trace) increases showing detuning of resonance due to heating.

tuning coefficient of 0.1 nm/°C and a minimum current tuning coefficient of 3 pm/mA. Due to the limitation of the OSA resolution, such a small tuning step could not be captured. The smallest observed tuning step of 50 pm is displayed in Fig. 3(a). The temperature was varied to tune the pump signal from higher to lower wavelengths. Throughout the wavelength tuning process, the Stokes power level was mostly stable, as can be seen from Fig. 3(a). However, a drop in the Stokes power level was witnessed twice during the tuning experiment, which could occur due to detuning of the new pump laser wavelength from the available WGM resonance. For both instances, decreasing the TDFA power by <3 mW recovered the original Stokes power level. Decreasing the pump power reduces the cavity temperature and thus blueshifts the resonance. Recovery of the Stokes power with a decrease in the pump power suggests that the pump wavelength was blue-detuned with respect to the WGM resonance and reducing the pump power realigned the pump and WGM mode. While fluctuations in the Stokes power during wavelength tuning can occur due to the misalignment of the new pump laser wavelength from the cavity resonance, stability of the Stokes power at a fixed pump wavelength depends on the detuning of the resonance from the fixed pump wavelength position due to variation in the cavity temperature.

For a silica microresonator, variation in the intracavity power changes the cavity temperature, which results in redshift or blueshift of resonances depending on whether the temperature is increased or decreased. The tuning of the resonance frequency while keeping the pump frequency fixed, therefore, affects the stability of the generated Stokes. However, stable Stokes can occur when the pump and the Stokes are blue- and redshifted with respect to their respective resonances [49]. To study the power stability of the Brillouin laser, we fixed the pump laser wavelength and measured the backscattered spectra at regular time intervals, and we plotted the power of the backreflected Stokes and transmitted pump on detectors as a function of time [see Fig. 3(b)]. From Fig. 3(b) it is evident that the Stokes power was stable for over 80 min, which is also seen from the optical spectra traces for the backscattered signal. The drop in Brillouin laser power after 80 min can be recovered by varying the pump power/wavelength, as observed during tuning study, or it can recover itself from a low-power to a high-power state as the cavity resonances realign with the pump and Stokes due to temperature stabilization (see Appendix). The recovery is illustrated in the Appendix where a growth in Stokes signal with time and its eventual stability was recorded for the same pump wavelength and also at a different one. We repeated the stability study at a different pump wavelength within the tuning range and observed stable Stokes generation for more than 90 min for a different pump position.

Linewidth measurement: Linewidth of a Brillouin laser can be determined by performing a self-heterodyne measurement on the first-order Stokes [29,50,51] or by operating the Brillouin laser in the multi-Stokes regime and observing the radiofrequency (RF) spectrum of the beat signal of the first- and third-order Stokes generated in the backward direction [24,30]. In our study, we measure the Brillouin laser linewidth by operating in the multi-Stokes regime and beating the first- and third-order Stokes. Earlier studies on the noise dynamics of cascaded Brillouin lasers have shown that the linewidth of the beat signal of two Stokes orders is the sum of the linewidths of participating Stokes tones [24,52]. We obtain the Brillouin laser linewidth by measuring the RF spectrum of the beat signal of the first- and third-order Stokes signals. The linewidths $\Delta\nu_1$ and $\Delta\nu_3$ of the first- and third-order Stokes,

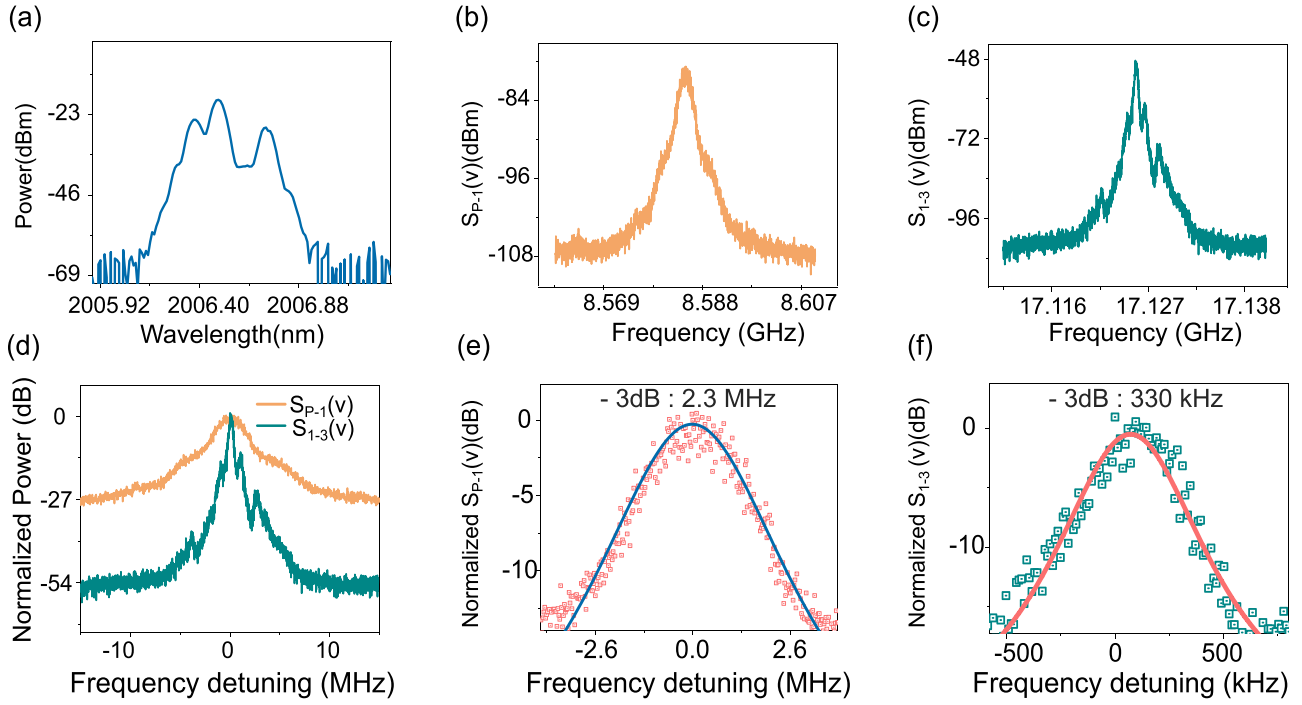

FIG. 4. Beat spectrum study: (a) Backscattered OSA spectrum showing pump, first-, and third-order Stokes signal. (b) RF-spectrum of beat signal between backscattered pump and first-order Stokes. (c) RF-spectrum of beat signal between first-order and third-order Stokes signal. (d) Normalized and centered plots of (b) and (c) showing that the 17.12 GHz beat spectrum is much narrower than the 8.58 GHz spectrum. Panels (e) and (f) are Lorentzian fits of 8.58 GHz and 17.12 GHz signals, respectively.

respectively, are then obtained by using the following relation between the linewidth ($\Delta\nu_{1-3}$) of the first- and third-order beat signal, and the powers P_1 and P_3 of the first- and third-order Stokes, respectively [24,52]:

$$\Delta\nu_1 = \frac{\Delta\nu_{1-3}}{1+\frac{P_1}{3P_3}}, \tag{3}$$

$$\Delta\nu_3 = \frac{\Delta\nu_{1-3}}{1+\frac{3P_3}{P_1}}, \tag{4}$$

and

$$\Delta\nu_{1-3} = \Delta\nu_1 + \Delta\nu_3. \tag{5}$$

The above equations imply that higher power of the first-order Stokes yields a narrower linewidth. We measure the RF spectrum [$S_{1-3}(\nu)$] of the beat signal of the first- and third-order Stokes for microspheres with slightly varying diameters (330 ± 6 μm), and we found $\Delta\nu_{1-3}$ to be ∼200 kHz.

Figure 4 shows the measured optical and RF spectra for a microsphere of diameter 324 μm. We employed the same experimental setup as shown in Fig. 2(a), where we did not close the feedback loop and sent the 90% reflected signal to an RF-spectrum analyser (Rhode and Schwarz) through a high-speed detector (12 GHz bandwidth) and an RF-amplifier with a gain of 25 dB over 18–32 GHz. The optical spectrum was simultaneously monitored at the 10% port of the splitter with the OSA. Figure 4(a) shows the measured optical spectrum demonstrating generation of the first- and third-order Stokes at a pump power of ∼120 mW. From the measured RF spectrum, we found that the beat signal between the backscattered pump and Stokes [$S_{P-1}(\nu)$] appears at 8.58 GHz [Fig. 4(b)] and the beat between first- and third-order Stokes signals [$S_{1-3}(\nu)$] is centered at 17.125 GHz [Fig. 4(c)]. To compare the bandwidths of $S_{P-1}(\nu)$ and $S_{1-3}(\nu)$, we normalize the two RF spectra and plot them in Fig. 4(d) as a function of detuning from their respective center frequencies. From the RF spectra in Fig. 4(d), we note that the $S_{1-3}(\nu)$ signal is much narrower than $S_{P-1}(\nu)$. Figures 4(e) and 4(f) plot the zoomed versions of Figs. 4(b) and 4(c), respectively, as a function of detuning along with the Lorentzian fits. From the fits, we obtain −3 dB linewidths of 2.3 MHz and 330 kHz for $S_{P-1}(\nu)$ and $S_{1-3}(\nu)$, respectively. To obtain $\Delta\nu_1$ and $\Delta\nu_3$ from $S_{1-3}(\nu)$, we calculate the ratio P_1/P_3 of the first- and third-order Stokes powers from the OSA spectrum in Fig. 4(a) and obtain a value of 4.33 for P_1/P_3. Using P_1/P_3 in Eqs. (3) and (4), we estimate $\Delta\nu_1$ and $\Delta\nu_3$ to be 135 and 194 kHz, respectively. The estimated Brillouin laser linewidth of 135 kHz is nearly 15 times smaller than the linewidth (2 MHz) of the pump laser. Fiber-based 2 μm Brillouin laser has been demonstrated in a 14-m-long standard single-mode silica fiber with a threshold of 1 W [37]. Exploiting high-Q resonances in a microsphere reduces the lasing threshold to 35 mW, resulting in a nearly 30-fold reduction in lasing threshold due to cavity enhancement.

In conclusion, we have demonstrated a low-threshold, tunable 2 μm microresonator Brillouin laser with stable output exploiting whispering gallery mode resonances in a silica microsphere. Using feedback of the backscattered signal, we generate first-, second-, and third-order Stokes signals with threshold powers of 35, 60, and 104 mW, respectively. We demonstrate a Brillouin laser with wavelength tunability of 1.8 nm, which is limited by the tuning range of the pump laser, while keeping a tuning resolution ∼10 pm and stable

laser output power at a fixed wavelength for over an hour. Although the FSR of the fundamental mode of the microsphere is ∼200 GHz, we exploit the closely spaced higher-order modes in a microsphere to achieve a tuning step much smaller than the Brillouin shift and FSR of the optical modes.

Microresonator-based Brillouin scattering has been used to demonstrate important applications like Brillouin-induced transparency and slow-light at 1550 nm [53], and recently it was used to pump frequency combs in the direction of the generated Stokes in the 1.55 μm [49,54] and 2 μm wavelength region [39]. Feeding back the Stokes using a fiber ring not only reduces the threshold for Brillouin lasing and the intracavity pumped Kerr comb but also reduces the noise of comb lines and allows tunability of the Brillouin laser and comb due to resonance shift in the composite cavity consisting of a microsphere and a fiber ring [39]. Microresonator Brillouin lasers in the 2 μm region therefore open up opportunities for generating low-power Kerr and soliton combs with reduced noise.

The Brillouin laser linewidth depends on cavity Q, Stokes power, and thermal fluctuations of cavity resonance according to [26]

$$\Delta\nu_{ST} = \frac{\hbar\omega^3}{4\pi Q_P Q_S P}(1 + n_T + N_T), \tag{6}$$

where n_T and N_T represent the thermal quanta of the mechanical and optical fields, respectively, $Q_{P,S}$ is the pump (Stokes) resonance quality factor, P is the Stokes power, and ω is the angular frequency of the Stokes signal. Taking temperature $T = 300$ K and $\nu_B = 8.57$ GHz, we found n_T to be 728. From Fig. 4(a), we obtain laser power $P = 0.14$ mW (scaled to 100% from the 10% OSA trace). Using $\frac{\omega}{2\pi} = 149.14$ THz and the measured value of quality factors $Q_{P,S} \sim 2$ million in Eq. (6), we obtain $\Delta\nu_{ST} = 90$ kHz, which is close to our experimentally obtained linewidth of 135 kHz. Further reduction in the linewidth can be achieved by improving the Q-factor and locking the pump laser to the cavity resonance using servo control, which reduces the thermal fluctuation induced detuning of the cavity resonance from the pump wavelength and thus allowing improved linewidth. The absorption limited Q-factor of silica at 2 μm is $Q = \frac{2\pi n_{\text{eff}}}{\lambda\alpha} = 2.25 \times 10^8$. In our study, the Q-factor is therefore not limited by large intrinsic absorption at 2 μm and there is a scope to further increase the Q-factor to reduce the Brillouin laser linewidth. One possible reason for the lower Q-factor in our measurements could be the exposure of the measurement setup to high humidity due to the local climatic conditions. In [55], it was observed that adsorption of water can lead to more than a 20% reduction in the Q-factor within a few minutes of fabrication, and therefore setting up such experiments in dry-gas-filled chambers is preferred. Degradation of the Q-factor due to adsorption of water increases at longer wavelengths [56], which may have resulted in further lowering of the Q-factor in our measurements. Although our experiments were conducted without the benefits of a dry environment and locking of pump to cavity resonance, we have demonstrated a Brillouin laser with a threshold of 35 mW (almost 30 times lower than that for a Brillouin fiber laser of similar length) and a narrow linewidth of 135 kHz along with a 1.8 nm tunability and >90 min of stability. In future, conducting the experiments in a dry gas-filled enclosure by locking the pump laser to the cavity resonance and operating at high pump powers will help in realizing much narrower linewidth 2 μm microresonator Brillouin lasers. This work opens up opportunities for exciting soliton and Kerr combs, and Brillouin induced transparency in the 2 μm wavelength region enabling dual-comb spectroscopy of atmospheric gases such as CO_2 and CO [57], signal processing for optical communications, and sources for gravitational wave detection.

R.P. proposed and designed the experiments. K.P. and S.P. fabricated the microsphere and taper, and conducted the experiments. K.P. conducted the calculations of optical and acoustic modes, and other modal overlap calculations using COMSOL. All the authors analyzed the data. R.P. wrote the manuscript with inputs from K.P. and S.P. R.P. supervised the project.

K.P. and S.P. contributed equally to this work.

APPENDIX: POWER STABILITY AND RECOVERY OF BRILLOUIN LASER

In Fig. 3(b) the Stokes power was stable for about 80 min and then the power dropped by more than 40 μW. In this case, the pump wavelength was centered at 2008.26 nm. The drop in Stokes power can be related to the following. The thermally stable configuration for Brillouin lasing in a resonance cavity is to have the pump signal blue-detuned and the Stokes signal red-detuned from their respective resonances [49]. Once this balance is disturbed, due to heating of the cavity as the pump and Stokes signals undergo many round trips for a long time [80 min for Fig. 3(b)], the signals become misaligned with respect to the now-shifted cavity resonances, leading to the drop in Stokes power. However, we found that even if the signals migrate from the "locked" position, it can always come back to a stable position. This is illustrated in Fig. 5(a). For the same pump wavelength at which the cavity went out of position after 80 min in Fig. 3(b) of the manuscript, we can see that the Stokes power grows with time for 40 min, and then stabilizes and stays at the same position for about an hour. We did not monitor the transmitted power while recording these data. However, we repeated the experiment at a different pump wavelength within the tuning range shown in Fig. 3(a) of the manuscript, this time monitoring the transmitted power as well. The fact that we again observed a rise and stabilization of Stokes power [Fig. 5(b)] shows that even in positions when the resonances and the signals become misaligned, stable configurations can always be recovered with time.

Determination of optical and mechanical modes through COMSOL and threshold calculation

To model the optical and mechanical modes, we referred to the work in [43], where a detailed tutorial is given to simulate the optical and mechanical modes in any geometry. We develop the code for a silica microsphere. We established a model based on a silica microsphere of diameter $d = 330$ μm for a pump wavelength of $\lambda_P = 2007.86$ nm and Stokes wavelength of $\lambda_S = 2007.92$ nm. The transverse electric field profiles (normalized) of the obtained pump, Stokes,

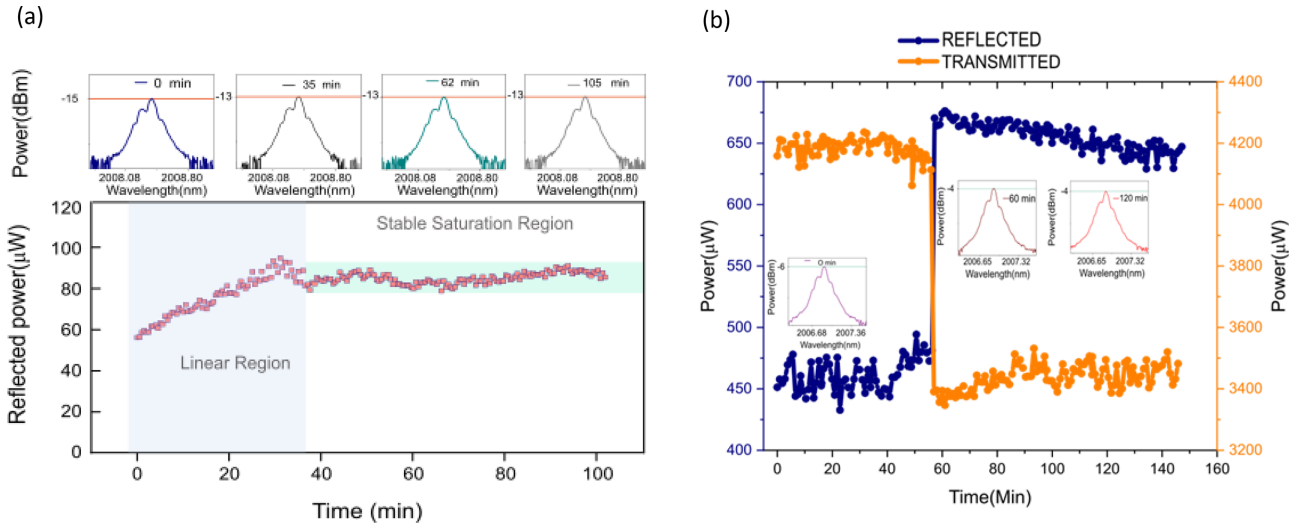

FIG. 5. (a) At a pump wavelength of 2008.26 nm, same as Fig. 3(b) in the manuscript, gradual growth and stable saturation of the Stokes signal achieved for greater than 60 min (demonstrating yet again how a system is brought to a stable configuration with high Stokes power despite starting with low power Stokes in an unstable configuration. (b) Reflected and transmitted power corresponding to stability study performed at a different wavelength.

and acoustic mode along with their respective azimuthal mode numbers are displayed in Fig. 6.

Calculation of Brillouin lasing threshold in a Whispering Gallery resonator has been done using different expressions in different studies. In [58], the expression used is

$$W_{\text{th}} = W_{\text{th}}^{0}\left(\frac{1+\zeta}{F}\right), \tag{A1a}$$

$$W_{\text{th}}^{0} = \frac{2\pi^3 n^2 V_P}{g Q_P Q_S \lambda_P^2}, \tag{A1b}$$

$$F = \frac{V_P \langle \psi_{1p}\psi_{1s}\phi_0\rangle^2}{\langle \psi_{1p}^2\rangle\langle \psi_{1s}^2\rangle\langle \phi_0^2\rangle}. \tag{A1c}$$

Here W_{th} is the threshold power for Brillouin lasing, V_P is the pump mode volume, g is the Brillouin gain coefficient, $Q_{p,s}$ is the quality factor of the pump (Stokes) resonance, λ_p is the pump wavelength, and F is defined as the modal overlap, with ψ_{1p}, ψ_{1s}, and ϕ_0 being the pump, Stokes, and the acoustic wave field profiles, respectively. ζ is a tailing function which can be ignored to be zero. The angular brackets ($\langle\rangle$) are used to denote an integral over the resonator volume.

On the other hand, the threshold power value in [27] is defined as

$$P_{\text{th}} = \frac{\pi^2 n^2 V_{\text{eff}}}{g_b Q_p Q_b \lambda_p \lambda_b}, \tag{A2}$$

where g_b is the gain coefficient, and λ_b is the Stokes wavelength, with Q_b being the Stokes quality factor. We found that using the definition $V_{\text{eff}} = V_p/F$, both Eqs. (A1) and (A2) are consistent. This is even more apparent in [28], where a slightly different form for the threshold power is used,

$$P_{\text{threshold}} = \left(\frac{\pi^2 n^2 V}{B g \lambda_p \lambda_s Q_p Q_s}\right)\left(\frac{1}{1+\frac{Q_m \Lambda_m}{2\pi r}}\right). \tag{A3}$$

Here, V is the pump mode volume and B is the modal overlap. This expression also includes the effect of mechanical quality factor Q_m, and the mechanical wavelength Λ_m on the Brillouin lasing threshold. The radius of the resonator is denoted as r. After making sure that Eq. (A3) is consistent

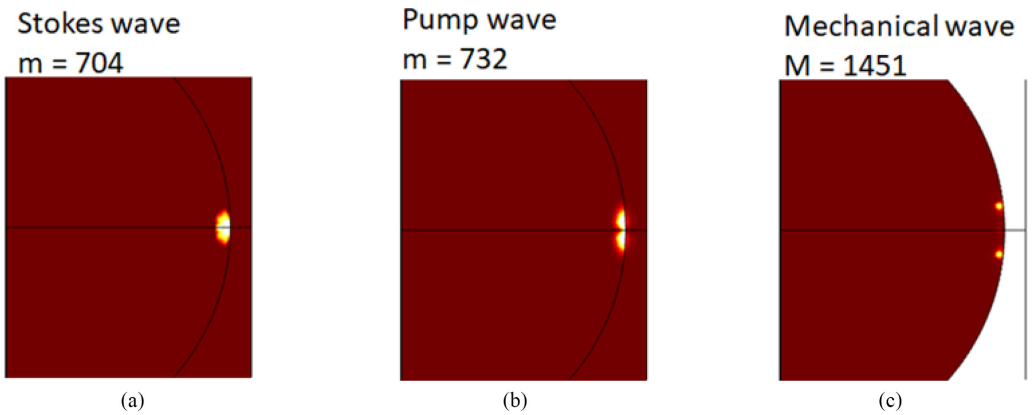

FIG. 6. Mode profiles of (a) Stokes, (b) pump, and (c) mechanical mode obtained through COMSOL simulation.

with (A1) and (A2), we use (A3) to calculate the threshold power. We performed COMSOL simulations and used Eq. (A3) to obtain the threshold value. Using COMSOL, we found an acoustic mode at 8.57 GHz. We got an effective mode volume of 4.33×10^{-14} m^3 ($V_P = 3.46 \times 10^{-17}$ m^3 and $B = 0.001$). For $g = 4.55 \times 10^{-12}$ m/W, we referred to [36], where the g was estimated for SMF at 2 μm. To calculate Q_m, we used the typical Brillouin gain bandwidth of 15 MHz [44] for SMF at 2 μm and the frequency of 8.57 GHz and we got a value of 571. Using all this in Eq. (A3), we obtained a threshold of ∼9 mW. The measured threshold of 40 mW is nearly four times higher than the estimated threshold. Equation (A3) assumes that the pump and Stokes are centered at the resonance frequency of their respective resonances. We attribute the higher value of the measured threshold to the detuning of the pump and Stokes from their respective resonances to achieve thermal equilibrium [49], as also mentioned above.

[1] D. P. Kapasi, J. Eichholz, T. McRae, R. L. Ward, B. J. J. Slagmolen, S. Legge, K. S. Hardman, P. A. Altin, and D. E. McClelland, Tunable narrow-linewidth laser at 2 μm wavelength for gravitational wave detector research, Opt. Express **28**, 3280 (2020).

[2] G. L. Mansell, T. G. McRae, P. A. Altin, M. J. Yap, R. L. Ward, B. J. J. Slagmolen, D. A. Shaddock, and D. E. McClelland, Observation of squeezed light in the 2 μm region, Phys. Rev. Lett. **120**, 203603 (2018).

[3] M. J. Yap, D. W. Gould, T. G. McRae, P. A. Altin, N. Kijbunchoo, G. L. Mansell, R. L. Ward, D. A. Shaddock, B. J. J. Slagmolen, and D. E. McClelland, Squeezed vacuum phase control at 2 μm, Opt. Lett. **44**, 5386 (2019).

[4] Z. Li, A. M. Heidt, J. M. O. Daniel, Y. Jung, S. U. Alam, and D. J. Richardson, Thulium-doped fiber amplifier for optical communications at 2 μm, Opt. Express **21**, 9289 (2013).

[5] Z. Du, S. Zhang, J. Li, N. Gao, and K. Tong, Mid-infrared tunable laser-based broadband fingerprint absorption spectroscopy for trace gas sensing: A review, Appl. Sci. **9**, 338 (2019).

[6] S. D. Jackson, Towards high-power mid-infrared emission from a fibre laser, Nat. Photon. **6**, 423 (2012).

[7] S. W. Henderson, P. J. M. Suni, C. P. Hale, S. M. Hannon, J. R. Magee, D. L. Bruns, and E. H. Yuen, Coherent laser radar at 2 μm using solid-state lasers, IEEE Trans. Geosci. Remote Sens. **31**, 4 (1993).

[8] D. J. Richardson, Filling the light pipe, Science **330**, 327 (2010).

[9] P. J. Winzer, Beyond 100G ethernet, IEEE Commun. Mag. **48**, 26 (2010).

[10] A. D. Ellis, J. Zhao, and D. Cotter, Approaching the non-linear shannon limit, J. Lightwave Technol. **28**, 423 (2009).

[11] F. Gunning and B. Corbett, Time to open the 2-μm window? Opt. Photon. News **30**, 42 (2019).

[12] N. V. Wheeler, T. D. Bradley, J. R. Hayes, M. A. Gouveia, S. Liang, Y. Chen, S. R. Sandoghchi, S. M. Abokhamis Mousavi, F. Poletti, M. N. Petrovich *et al.*, Low-loss kagome hollow-core fibers operating from the near-to the mid-IR, Opt. Lett. **42**, 2571 (2017).

[13] B. Shapiro, R. X. Adhikari, O. Aguiar, E. Bonilla, D. Fan, L. Gan, I. Gomez, S. Khandelwal, B. Lantz, T. MacDonald *et al.*, Cryogenically cooled ultra low vibration silicon mirrors for gravitational wave observatories, Cryogenics **81**, 83 (2017).

[14] Q. Zhang, Y. Hou, X. Wang, W. Song, X. Chen, W. Bin, J. Li, C. Zhao, and P. Wang, 5 W ultra-low-noise 2 μm single-frequency fiber laser for next-generation gravitational wave detectors, Opt. Lett. **45**, 4911 (2020).

[15] J. Li, Y. Liu, Y. Meng, K. Xu, J. Du, F. Wang, Z. He, and Q. Song, 2- μm wavelength grating coupler, bent waveguide, and tunable microring on silicon photonic MPW, IEEE Photon. Technol. Lett. **30**, 471 (2018).

[16] S. P. Smith, F. Zarinetchi, and S. Ezekiel, Narrow-linewidth stimulated Brillouin fiber laser and applications, Opt. Lett. **16**, 393 (1991).

[17] I. Remer and A. Bilenca, Background-free Brillouin spectroscopy in scattering media at 780 nm via stimulated Brillouin scattering, Opt. Lett. **41**, 926 (2016).

[18] I. Remer and A. Bilenca, High-speed stimulated Brillouin scattering spectroscopy at 780 nm, APL Photon. **1**, 061301 (2016).

[19] Z. Bai, R. J. Williams, O. Kitzler, S. Sarang, D. J. Spence, Y. Wang, Z. Lu, and R. P. Mildren, Diamond Brillouin laser in the visible, APL Photon. **5**, 031301 (2020).

[20] K. S. Abedin, Brillouin amplification and lasing in a single-mode As_2Se_3 chalcogenide fiber, Opt. Lett. **31**, 1615 (2006).

[21] R. Pant, C. G. Poulton, D.-Y. Choi, H. Mcfarlane, S. Hile, E. Li, L. Thevenaz, B. Luther-Davies, S. J. Madden, and B. J. Eggleton, On-chip stimulated Brillouin scattering, Opt. Express **19**, 8285 (2011).

[22] R. Pant, E. Li, D.-Y. Choi, C. G. Poulton, S. J. Madden, B. Luther-Davies, and B. J. Eggleton, Cavity enhanced stimulated Brillouin scattering in an optical chip for multiorder stokes generation, Opt. Lett. **36**, 3687 (2011).

[23] I. V. Kabakova, R. Pant, D.-Y. Choi, S. Debbarma, B. Luther-Davies, S. J. Madden, and B. J. Eggleton, Narrow linewidth Brillouin laser based on chalcogenide photonic chip, Opt. Lett. **38**, 3208 (2013).

[24] S. Gundavarapu, G. M. Brodnik, M. Puckett, T. Huffman, D. Bose, R. Behunin, J. Wu, T. Qiu, C. Pinho, N. Chauhan *et al.*, Sub-hertz fundamental linewidth photonic integrated Brillouin laser, Nat. Photon. **13**, 60 (2019).

[25] N. T. Otterstrom, R. O. Behunin, E. A. Kittlaus, Z. Wang, and P. T. Rakich, A silicon Brillouin laser, Science **360**, 1113 (2018).

[26] J. Li, H. Lee, T. Chen, and K. J. Vahala, Characterization of a high coherence, Brillouin microcavity laser on silicon, Opt. Express **20**, 20170 (2012).

[27] H. Lee, T. Chen, J. Li, K. Y. Yang, S. Jeon, O. Painter, and K. J. Vahala, Chemically etched ultrahigh-q wedge-resonator on a silicon chip, Nat. Photon. **6**, 369 (2012).

[28] M. Tomes and T. Carmon, Photonic micro-electromechanical systems vibrating at X-band (11-GHz) rates, Phys. Rev. Lett. **102**, 113601 (2009).

[29] W. Loh, A. A. S. Green, F. N. Baynes, D. C. Cole, F. J. Quinlan, H. Lee, K. J. Vahala, S. B. Papp, and S. A. Diddams, Dual-microcavity narrow-linewidth Brillouin laser, Optica **2**, 225 (2015).

[30] J. Li, H. Lee, and K. J. Vahala, Microwave synthesizer using an on-chip Brillouin oscillator, Nat. Commun. **4**, 2097 (2013).

[31] N. Chauhan, A. Isichenko, K. Liu, J. Wang, Q. Zhao, R. O. Behunin, P. T. Rakich, A. M. Jayich, C. Fertig, C. W. Hoyt *et al.*, Visible light photonic integrated Brillouin laser, Nat. Commun. **12**, 4685 (2021).

[32] S. Jiang, C. Guo, K. Che, Z. Luo, T. Du, H. Fu, H. Xu, and Z. Cai, Visible raman and Brillouin lasers from a microresonator/ZBLAN-fiber hybrid system, Photon. Res. **7**, 566 (2019).

[33] R. I. Woodward, E. J. R. Kelleher, S. V. Popov, and J. R. Taylor, Stimulated Brillouin scattering of visible light in small-core photonic crystal fibers, Opt. Lett. **39**, 2330 (2014).

[34] K. Hu, I. V. Kabakova, T. F. S. Büttner, S. Lefrancois, D. D. Hudson, S. He, and B. J. Eggleton, Low-threshold Brillouin laser at 2 μm based on suspended-core chalcogenide fiber, Opt. Lett. **39**, 4651 (2014).

[35] X. Wang, P. Zhou, X. Wang, H. Xiao, and L. Si, Multi-wavelength Brillouin-thulium fiber laser, IEEE Photon. J. **6**, 1 (2013).

[36] A. Mishra and R. Pant, Efficient Brillouin lasing and multi-stokes generation at 2004 nm, OSA Continuum **2**, 2826 (2019).

[37] Y. Luo, Y. Tang, J. Yang, Y. Wang, S. Wang, K. Tao, L. Zhan, and J. Xu, High signal-to-noise ratio, single-frequency 2 μm Brillouin fiber laser, Opt. Lett. **39**, 2626 (2014).

[38] K. Pathak and R. Pant, Demonstration of Brillouin Lasing in a Silica Microsphere at 2 μm, in *Nonlinear Photonics*, (Optica, 2022), p. NpM2E–1.

[39] K. Pathak and R. Pant, Intracavity pumped tunable low threshold mid-IR Kerr comb at 2 μm, Optica Open, doi:10.1364/opticaopen.22736693.v1 (2023).

[40] K. Shiraki, M. Ohashi, and M. Tateda, Sbs threshold of a fiber with a Brillouin frequency shift distribution, J. Lightwave Technol. **14**, 50 (1996).

[41] G. Bahl, J. Zehnpfennig, M. Tomes, and T. Carmon, Stimulated optomechanical excitation of surface acoustic waves in a microdevice, Nat. Commun. **2**, 403 (2011).

[42] G. Bahl, X. Fan, and T. Carmon, Acoustic whispering-gallery modes in optomechanical shells, New J. Phys. **14**, 115026 (2012).

[43] G. S. Wiederhecker, P. Dainese, and T. P. Mayer Alegre, Brillouin optomechanics in nanophotonic structures, APL Photon. **4**, 071101 (2019).

[44] M. Deroh, J.-C. Beugnot, K. Hammani, C. Finot, J. Fatome, F. Smektala, H. Maillotte, T. Sylvestre, and B. Kibler, Comparative analysis of stimulated Brillouin scattering at 2 μm in various infrared glass-based optical fibers, J. Opt. Soc. Am. B **37**, 3792 (2020).

[45] K. Hu, I. V. Kabakova, S. Lefrancois, D. D. Hudson, S. He, and B. J. Eggleton, Hybrid Brillouin/thulium multiwavelength fiber laser with switchable single-and double-Brillouin-frequency spacing, Opt. Express **22**, 31884 (2014).

[46] T. Yin, B.-M. Mao, Y. Wei, and D. Chen, Widely wavelength-tunable 2 μm Brillouin fiber laser incorporating a highly germania-doped fiber, Appl. Opt. **57**, 6831 (2018).

[47] S. B. Gorajoobi, G. S. Murugan, and M. N. Zervas, Efficient excitation and phase matching of fiber-coupled degenerate whispering gallery modes, J. Opt. Soc. Am. B **36**, 2452 (2019).

[48] A. A. Savchenkov, A. B. Matsko, V. S. Ilchenko, D. Strekalov, and L. Maleki, Direct observation of stopped light in a whispering-gallery-mode microresonator, Phys. Rev. A **76**, 023816 (2007).

[49] Y. Bai, M. Zhang, Q. Shi, S. Ding, Y. Qin, Z. Xie, X. Jiang, and M. Xiao, Brillouin-Kerr soliton frequency combs in an optical microresonator, Phys. Rev. Lett. **126**, 063901 (2021).

[50] O. Llopis, P.-H. Merrer, H. Brahimi, K. Saleh, and P. Lacroix, Phase noise measurement of a narrow linewidth CW laser using delay line approaches, Opt. Lett. **36**, 2713 (2011).

[51] Y. Wang, L. Yang, F. Yang, L. Xu, Z. Wu, T. Liu, D. Wu, L. Zhang, and S. Dai, Low-threshold and sub-kHz-linewidth Brillouin laser based on chalcogenide fiber at 2μm, J. Lightwave Technol. **40**, 7390 (2022).

[52] R. O. Behunin, N. T. Otterstrom, P. T. Rakich, S. Gundavarapu, and D. J. Blumenthal, Fundamental noise dynamics in cascaded-order Brillouin lasers, Phys. Rev. A **98**, 023832 (2018).

[53] C.-H. Dong, Z. Shen, C.-L. Zou, Y.-L. Zhang, W. Fu, and G.-C. Guo, Brillouin-scattering-induced transparency and non-reciprocal light storage, Nat. Commun. **6**, 6193 (2015).

[54] H. Zhang, T. Tan, H. J. Chen, Y. Yu, W. Wang, B. Chang, Y. Liang, Y. Guo, H. Zhou, H. Xia, Q. Gong, C. W. Wong, Y. Rao, Y. F. Xiao, and B. Yao, Soliton microcombs multiplexing using intracavity-stimulated Brillouin lasers, Phys. Rev. Lett. **130**, 153802 (2023).

[55] M. L. Gorodetsky, A. A. Savchenkov, and V. S. Ilchenko, Ultimate Q of optical microsphere resonators, Opt. Lett. **21**, 453 (1996).

[56] D. W. Vernooy, V. S. Ilchenko, H. Mabuchi, E. W. Streed, and H. J. Kimble, High-Q measurements of fused-silica microspheres in the near infrared, Opt. Lett. **23**, 247 (1998).

[57] E. Russell, A. A. Ruth, B. Corbett, and F. C. Garcia Gunning, Tunable dual optical frequency comb at 2 μm for CO_2 sensing, Opt. Express **31**, 6304 (2023).

[58] B. Sturman and I. Breunig, Brillouin lasing in whispering gallery micro-resonators, New J. Phys. **17**, 125006 (2015).